Model-Driven Scheduling of Nanocarriers: Application to an Anticancer Polymer Prodrug Administered Subcutaneously

Anne Rodallec, Randy Lee, Jingming Cao, Sophie Marolleau, Julien Nicolas, Sébastien Benzekry

Model-Driven Scheduling of Nanocarriers: Application to an Anticancer Polymer Prodrug Administered Subcutaneously

Anne Rodallec,[1,2] Randy Lee,[1] Jingming Cao,[3] Sophie Marolleau,[1,2] Julien Nicolas,[3,*] Sébastien Benzekry[1,*]

1. COMPutational pharmacology and clinical Oncology Department, Inria Sophia Antipolis – Méditerranée, Cancer Research Center of Marseille, Inserm UMR1068, CNRS UMR7258, Aix Marseille University UM105, Marseille, France

2. SMARTc, Cancer Research Center of Marseille, Inserm UMR1068, CNRS UMR7258, Aix Marseille University UM105, Marseille, France

3. Université Paris-Saclay, CNRS, Institut Galien Paris-Saclay, 91400 Orsay, France

The authors declare no conflict of interest.

*To whom correspondence should be addressed.

E-mail: julien.nicolas@universite-paris-saclay.fr (JN) and sebastien.benzekry@inria.fr (SB)

ABSTRACT

The limitations of chemotherapy (e.g., toxicities, limited efficacy) have led to the development of nanocarriers for drug delivery to improve pharmacokinetics (PK) and therapeutic outcomes. However, optimizing dosing regimens remains challenging. Moreover, since chemotherapy are mainly administered intravenously (IV), this results in patient discomfort and high treatment cost.

To address these issues, we used PK/pharmacodynamics (PD) modeling and applied it to subcutaneously (SC) injectable polymer prodrug based on paclitaxel (Ptx) and polyacrylamide (PAAm).

PK/PD studies were performed on MCF-7 tumor-bearing mice. The PK model was developed on IV Ptx and SC Ptx-PAAm data. The PD model was developed on control, IV Ptx, and SC Ptx-PAAm groups (15 mg/kg), and validated on an independent group (SC Ptx-PAAm 60 mg/kg). Optimal dosing regimens identified *in silico* were then validated *in vivo* with excellent agreement. A dosing regimen combining a loading dose and daily injections achieved a 60% complete response rate without added toxicity, outperforming prior results.

This is the first validated PK/PD model for nanocarriers, offering a framework for more effective, cost-efficient, and ethically refined drug development.

INTRODUCTION

Cancer remains a major concern due to its public health burden and subsequent economic impact [1]. As a result of population growth and aging, the number of new cancer cases is projected to rise by about 70% over the next two decades [2]. The majority of expected cancer deaths are from solid tumors, including lung, ovarian, and breast cancers. When surgery is not feasible or sufficient, or in advanced cases, chemotherapy — either alone or combined with other treatments — is commonly used. However, due to their unspecific distribution profile and toxic excipients, these treatments are consistently associated with high toxicities, and moderate efficacy. Furthermore, as most chemotherapies are administered intravenously, this contributes directly to patient discomfort. In addition, this increases the cost of cancer care, for instance due to long inpatient hospital stays, the need for qualified staff, the invasive nature of the administration protocol, and potential catheter failures and life-threatening infections [3].

Consequently, numerous strategies have been considered to enhance the therapeutic effect of anti-cancer drugs, with the aim of increasing tumor uptake and/or reducing side effects. Among them, drug-loaded nanocarriers and polymer-drug conjugates (also called polymer prodrugs) have been the focus of great attention [4–6]. These approaches can indeed increase water solubility as well as provide enhanced bioavailability, so that patients could benefit from an improved pharmacokinetic (PK) profile, resulting in a better efficacy / toxicity balance.

However, as nanocarriers and polymer prodrugs exhibit altered pharmacokinetics, standard therapeutic regimens must be reconsidered. Indeed, the conventional dosing schedules based on the maximum tolerated dose (MTD) were originally designed for free drugs with rapid clearance and systemic toxicity [7]. These may no longer be optimal and the investigation of new treatment dosing regimens is needed.

In this context, PK / pharmacodynamics (PD) modeling allows to create early-stage pharmacological digital twins (Figure 1), by exploring infinitely many scheduling possibilities in terms of dose, frequency and duration of treatment [8]. It also saves substantial time and cost, in addition to addressing ethical considerations. It consists in first modeling the relationship between the dose scheduling and the concentration or exposure (PK), and then model the association between exposure and response

(PD). Several types of models have been developed, either for biodistribution (e.g., drug delivery to the brain [9]), intra-tumor drug penetration [10], or physiologically-based-PK models to extrapolate the dose across species [11]. However, the ultimate outcome of this approach (i.e., anti-tumor effect), has rarely been modeled, let alone confronted with experimental data. While previous studies have explored the potential of combination therapies and optimized drug scheduling (e.g., dose, treatment duration) [12,13], they were never further validated with *in vivo* data for predicting the performance of different treatment regimens or demonstrated an improvement in anticancer outcomes.

Herein, we report the first experimental PK/PD model in oncology for nanocarriers, whose predictions of anticancer efficacy are validated *in vivo*, making it possible to optimize treatment regimens and obtain better therapeutic efficacy.

As a proof of concept, we apply this approach to the subcutaneous (SC) administration of a water-soluble paclitaxel-polyacrylamide (Ptx-PAAm) prodrug, whose preclinical development in mice has recently shown great promise [14]. SC administration is indeed considered to be a more convenient alternative for patients than IV administration [15,16], as the SC route is much less invasive than the intravenous (IV) route and home (self-)administration may become possible, thus increasing patient comfort, reducing hospitalization time as well as treatment costs [17]. Subcutaneously-injected, water-soluble Ptx-PAAm prodrugs (SC Ptx-PAAm) have shown no cutaneous toxicity despite the vesicant/irritant nature of Ptx, and was more effective under conventional dosing schedules than IV administration of Taxol, the commercial formulation of Ptx, which is a cornerstone in the treatment of metastatic breast cancer [18]. PAAm has been chosen for its biocompatibility, greater hydrophilicity than poly(ethylene glycol) and stealth properties, and is already used as a wrinkle filler.

To develop this PK/PD model, we implemented an integrative *in vivo / in silico* approach, using experimental data from SC Ptx-PAAm. An initial dataset was used to establish and train the model. We then demonstrated: (i) the validity of the model's predictions on a dose regimen distinct from the training dataset; (ii) its use for *in silico* treatment regimen exploration, and (iii) the *in vivo* validation of the model's predictions, ultimately leading to greater efficacy with no additional toxicity.

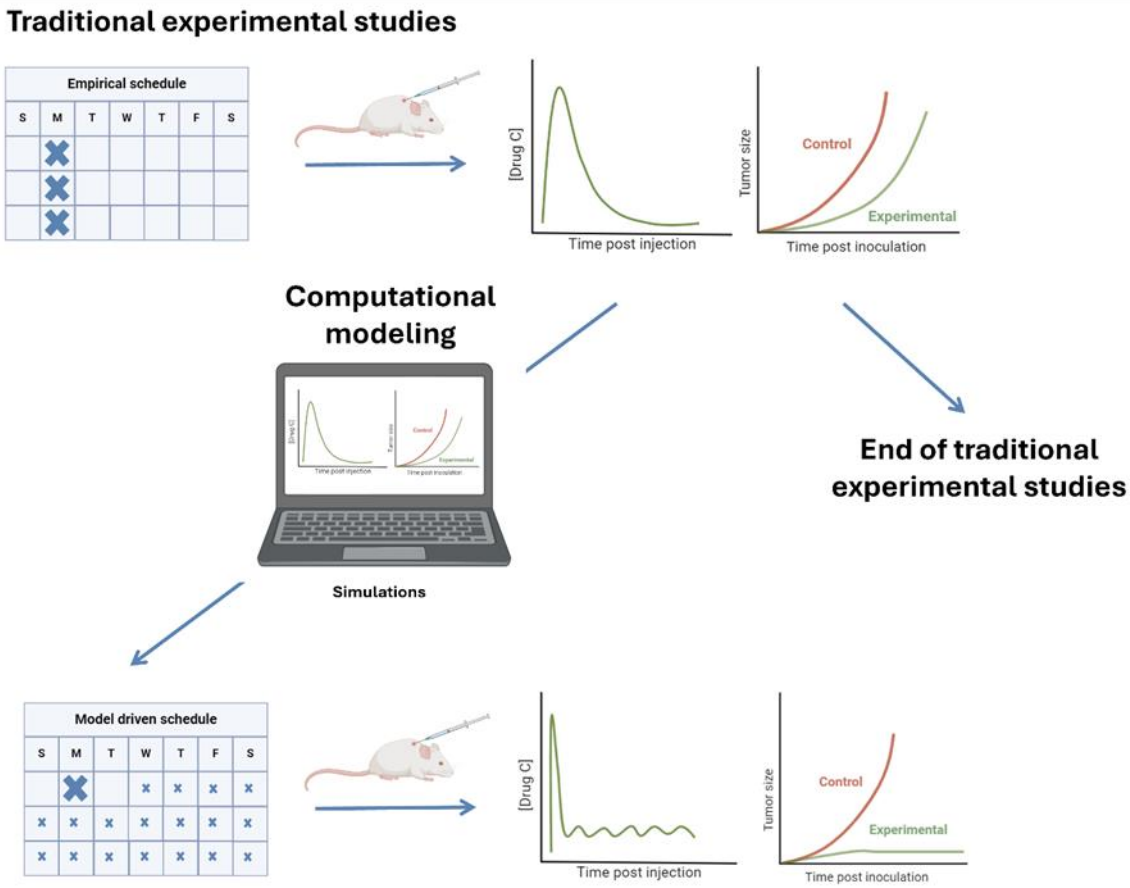

Figure 1. Schematic representation of the methodology. Using previously established PK/PD data, a mathematical model was developed and trained a subset of the data (training set), then validated on a separate set with a different dose. The model was subsequently used to simulate multiple dose regimens *in silico*, allowing for the selection of a reduced number of model-driven schedule candidates. Finally, the efficacy and toxicity of these candidates were evaluated *in vivo*.

RESULTS

The final structure of the PK/PD model is reported in Figure 2. It was developed sequentially using separate pharmacokinetic and pharmacodynamic *in vivo* studies from SC Ptx-PAAm in mice (see Materials and Methods). Multiple models were considered during model development. The final equations and all population parameter estimates are provided in the Supplementary Information (Equation S1 and Table S1).

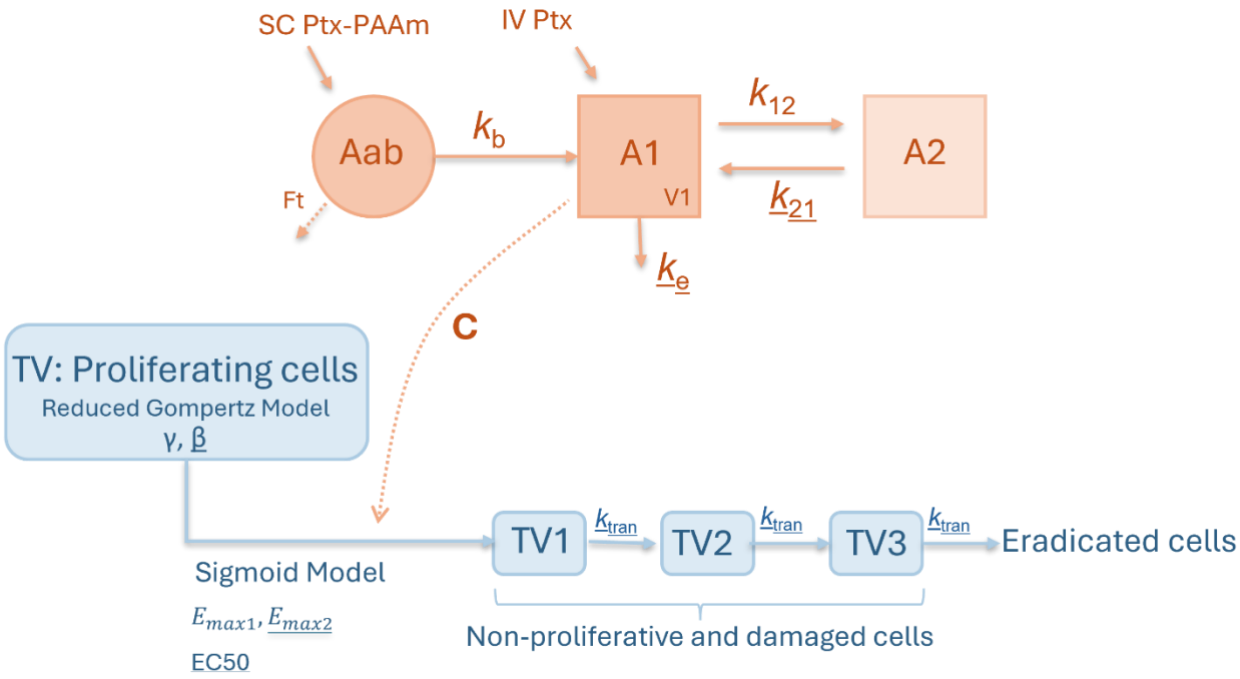

Figure 2. Structure of the final PK/PD model. In orange, the model structure of the two-compartment PK model for Ptx-PAAm, with an additional depot compartment for SC administration. The output is the free Ptx concentration (C), which acts as input in the PD model (in blue).

Pharmacokinetic modeling

The structural model was gradually built using *in vivo* data from IV Ptx and SC Ptx-PAAm treatment groups at 7 mg/kg with the following steps: (i) selecting the IV Ptx structural model and identifying the population PK parameters; (ii) developing an additional depot compartment for SC Ptx-PAAm and identifying specific parameters while keeping the Ptx population parameters fixed, and (iii) identifying all the population PK parameters simultaneously by combining the selected structural models. The final structural model for IV Ptx PK was a linear two-compartments model with first-order

elimination (central A_1 and peripheral A_2, exchange rates k_{12} and k_{21}, elimination rate k_e, Figure 2). SC administration of Ptx-PAAm was modeled by a depot (absorption) compartment Aab with bioavailability Ft and transfer rate to the central compartment k_b.

Goodness-of-fit was validated by visual and numerical analysis (Figure 3 and Supplementary Information Table S1) and no misspecification (i.e., 0% outlier proportions) was observed (Figure 3C). Thus, PK parameters were obtained from the PK model for all treatment groups and robustness of convergence was confirmed. The estimated apparent bioavailability was found to be in the same range as that calculated during non-compartmental PK analysis [14] (i.e., 36% *versus* 28%, respectively), as were the AUCs (i.e., 5160 ng/mL/h *versus* 4631 ng/mL/h and 1350 ng/mL/h *versus* 1299 ng/mL/h for IV Ptx and SC Ptx-PAAm, respectively). Therefore, the model was considered trustworthy, and it was used for further PK/PD modeling.

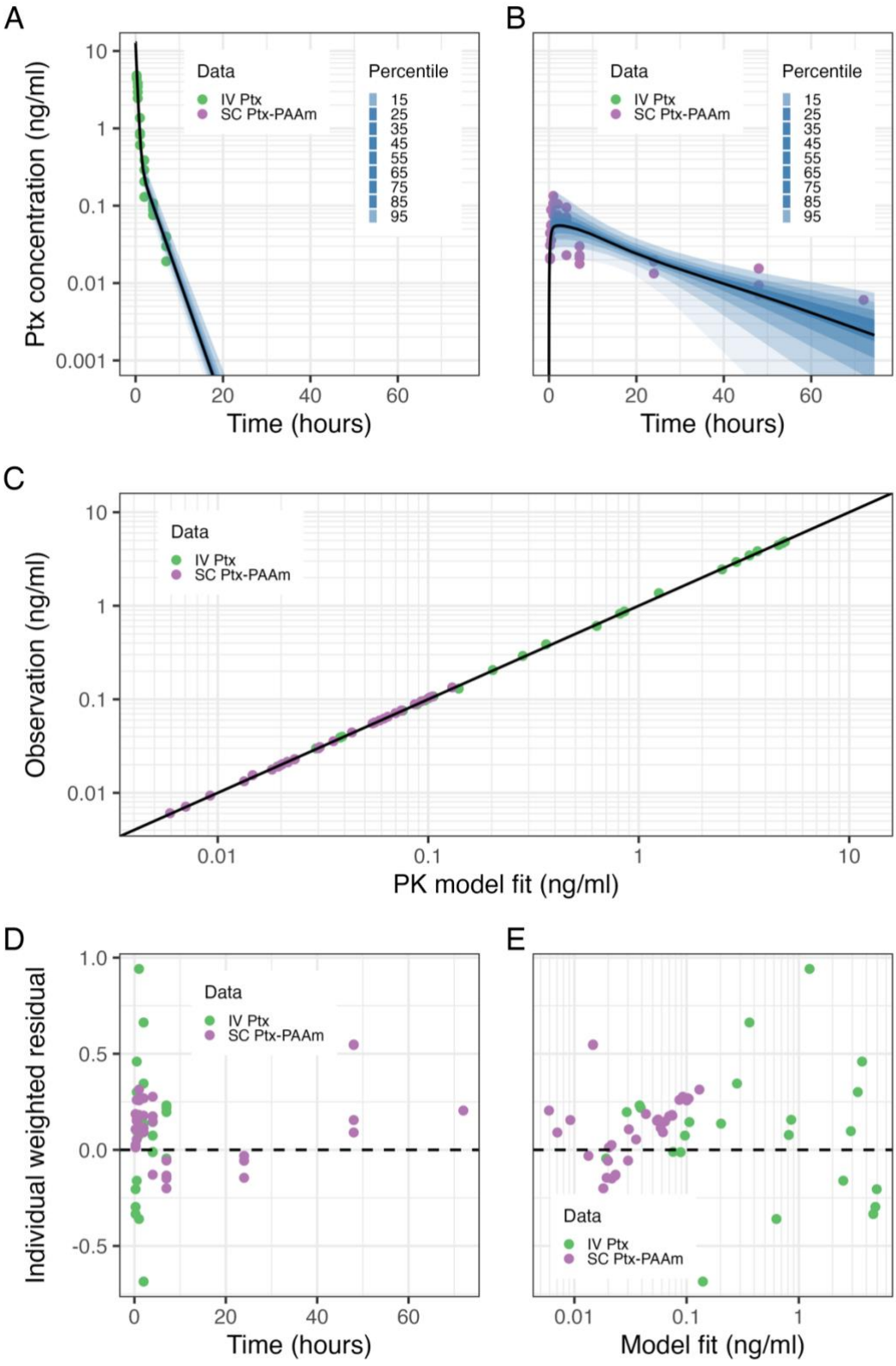

Figure 3. Population PK data and model. Observations IV Ptx and SC Ptx-PAAm at 7 mg/kg are represented by green and purple dots, respectively. (A-B) Prediction distributions from 500 simulations allow us to compare the observations (dots) with the theoretical inter-animal distribution of the predictions (blue areas). Black line represents the median over individuals. (C) Individual PK observations versus model fits. The black line represents the y = x equation. Dotted black lines represent the 95 % interval. (D-E) Scatter plots of the residuals between the observations and model fits.

Pharmacodynamics modeling

The efficacy of Ptx depends on its free concentration estimated by the PK model (C) (see Figure 2), assuming that Ptx damages tumor cells, eventually leading them to their elimination from the tumor volume after three consecutive damaged states (Simeoni model [19]). The model was refined using a sigmoid maximum drug effect function as well as a resistance model, allowing for greater efficacy for the first treatment (E_{max1}) compared to subsequent treatments (E_{max2})

The PD structural model was gradually built with the following steps: (i) untreated tumor growth models tested and calibrated with the negative control data (i.e., PAAm 60 mg/kg eq. Ptx); (ii) efficacy of Ptx on tumor growth, and (iii) resistance to Ptx using two additional treatment groups (i.e., IV Ptx 15 mg/kg and SC Ptx-PAAm 15 mg/kg eq. Ptx). The final model is depicted in Figure 2 and its equations are reported in Equation S1.

Based on goodness-of-fit and number of parameters, we selected the reduced Gompertz model as the most suitable model for untreated tumor growth, consistently with previous work [20]. Using the free Ptx concentration *C* outputted by the PK model as input of the PD efficacy model, the latter was first described using a Simeoni model [19]. It consists in three transit compartments representing damaged cells, unable to proliferate, but only removed from the tumor volume when reaching the last compartment (Figure 2). However, misspecifications in individual fits (Figure S1) were observed in 44% (i.e., 4 out of 9) and 11% (i.e., 1 out of 9) of individuals of IV Ptx 15 mg/kg and SC Ptx-PAAm 15 mg/kg eq. Ptx, respectively, leading us to refine the model. We thus implemented an E_{max} model (i.e., $\mathrm{E} = \frac{(E_{max} \cdot \mathrm{C})}{(\mathrm{EC50} + \mathrm{C})}$), that still yielded sub-optimal fits (Figure S1). The observed misspecification represented an overpredicted tumor growth after the first administration. We hypothesized that it could be due to a stronger anti-tumor effect for the first administration than in subsequent ones (i.e., resistance to treatment). To model this resistance, we used two distinct E_{max1} and E_{max2} values for the first and subsequent administrations, respectively, with $E_{max1} > E_{max2}$ (Equation S1). This effectively improved the goodness-of-fit in the training set (Figures S1 and S2).

The robustness of the final model was supported by the narrow confidence intervals in the visual predictive checks (Figure 4A, left column) where no misspecification in the structural and statistical models was observed. For the SC Ptx-PAAm 15 mg/kg eq.

Ptx group, minor dropouts (i.e., outliers) were observed at later stages because of animal exclusion when tumor reached a large volume (i.e., 2000 mm^3). The model could also capture inter-animal variability (Figure 4, middle column) as well as individual fits (Figure 4, right column) across untreated tumor growth and two formulations of Ptx (i.e., IV Ptx and SC Ptx-PAAm). In addition, parametric identifiability was good (Table S1), indicating that the training data was sufficient to calibrate the model.

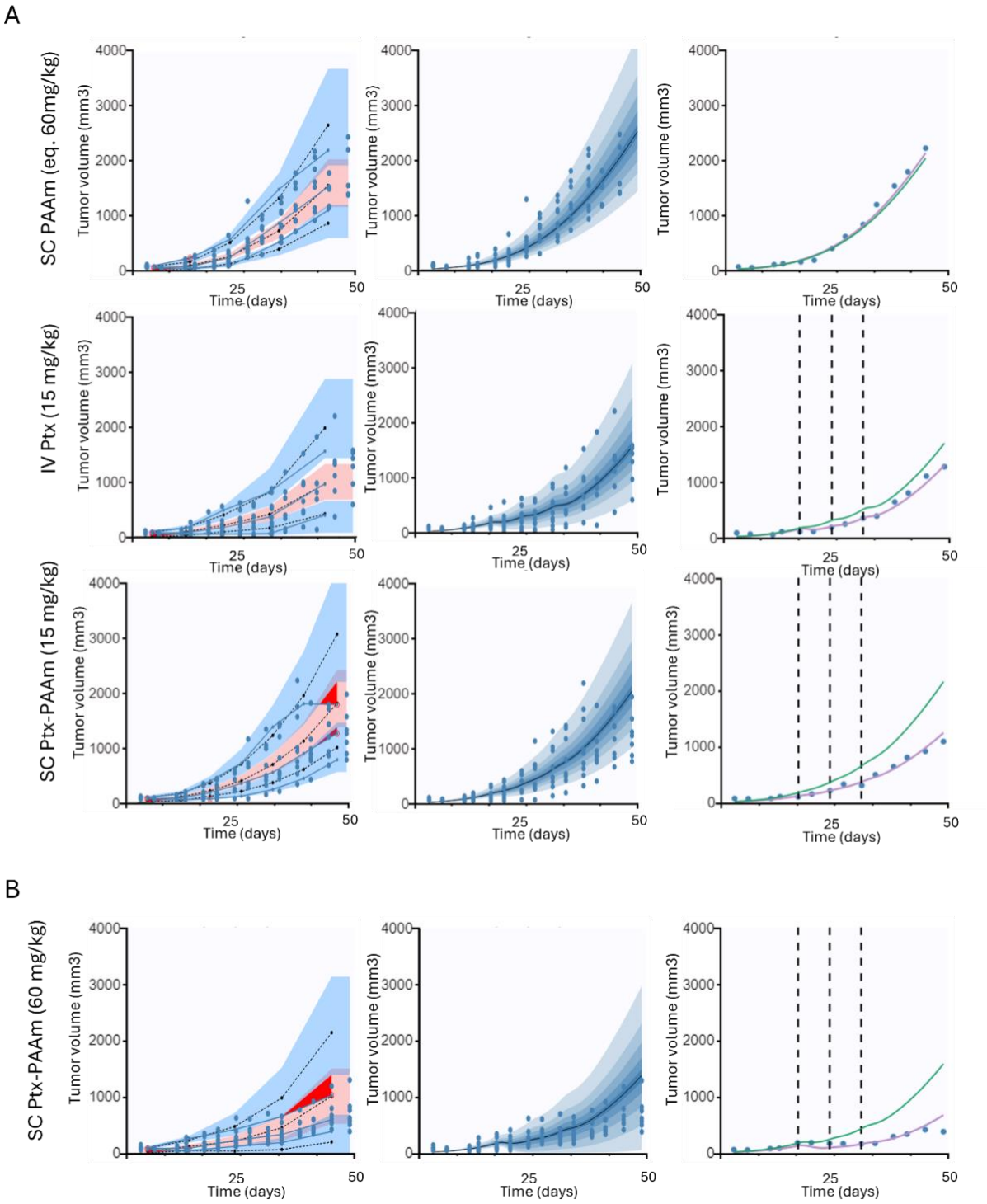

Figure 4. Diagnostic plots obtained from 500 simulations of the final PK/PD model on the training (A) and test (B) data set. VPCs (left column) assess goodness-of-fit for structural dynamics and inter-animal variability. Dotted black lines represent the predicted percentiles. Blue and pink areas represent the prediction interval. Blue dots represent observed data. Blue line represents the empirical percentiles. Outliers are represented by the red areas. Prediction distributions (middle column) allow us to compare the observations (blue dots) with the theoretical distribution of the predictions (blue areas). Black line represents the median over individuals. Individual fits (right column), chosen randomly for each

treatment group. Dotted black lines represent dosing times. Purple and green lines represent individual and population fits, respectively. Blue dots represent observed data.

PK/PD model validation

The SC Ptx-PAAm (60 mg/kg eq. Ptx) group was then used as an independent data to assess the model predictions. Fit-free predictions remained highly accurate at the individual level (Figure 4B and Figures S2), and captured inter-animal variability with only a slight overprediction at later time points (Figure 4B). This demonstrates the ability of the model to extrapolate to administration schedules not seen during training.

Once validated, we retrained the model on the entire data set (i.e., SC PAAm 60 mg/kg eq. Ptx as control group, IV Ptx 15 mg/kg, SC Ptx-PAAm 15 mg/kg eq. Ptx and SC Ptx-PAAm 60 mg/kg eq. Ptx) and used the resulting parameter estimates) for subsequent simulations (Table S2). Lower relative standard errors were observed (e.g., from 59.9 % to 40.1 % for $Emax_1$) (Tables S1 and S2), confirming the model refinement with more data. Of note, however, changes in the estimates of parameters $Emax_1$, (from 6.85 to 15.48), $Emax_2$ (from 2.51 to 13.8) and EC_{50} (from 156.1 to 462.7) were observed, due to correlations in the parameter estimates.

In silico exploration of dosing schedules

Simulations of the PK/PD model were conducted to explore a wide range of potential dosing schedules, using a study design involving 10 mice per group over 54 days. Seven of these dosing schedules were selected based on their safety and anticancer efficacy (Table 1). Group 1 was the benchmark reference, already evaluated in a previous work [14]. It consisted of equally dosed administrations once a week, for three weeks (total dose 180 mg/kg eq. Ptx). Pharmacokinetic simulations suggested that the total Ptx dose over 21 days could be safely tripled from 180 mg/kg to 540 mg/kg eq. Ptx. Indeed, the maximum observed concentration C_{max} for SC Ptx-PAAm 180 mg/kg eq. Ptx administration was lower than the previously measured C_{max} for IV Ptx 7 mg/kg administration (i.e., 1.7 µg/mL from Figure 5A Group 2, *versus* 4.7 µg/mL from [14]). The maximum single dose ever administered for SC Ptx-PAAm is 180 mg/kg eq. Ptx [14]. Therefore, any regimen involving a single dose exceeding this threshold was disregarded, and a minimal washout period of 48 h was imposed between successive administrations. PK/PD simulations revealed that, for a same total dose of 180 mg/kg

(Groups 1, 2 and 3), single administration (Group 2) led to a significantly greater efficacy compared to both daily (Group 3) and weekly (Group 1) dosing regimens (Figure 5B). This better efficacy lasted for 15 days, after which weekly and finally, daily administration (i.e., metronomic therapy [7]) took over. Since the *in silico* analysis above suggested a possible resistance to Ptx after the first administration, the interest of a loading dose followed by a maintenance dose (i.e., daily administration following the loading dose) (Group 4) was investigated and resulted in slightly weaker efficacy than daily administration (Figure 5B). Similar results were observed at a higher total dose (300 mg/kg) between Groups 5 (loading dose + maintenance treatment) and 6 (daily administration). Interestingly, a daily dose of 14.3 mkg/kg (Group 6) was found to efficiently control tumor growth (i.e., tumor growth plateaued in Figure 5B), suggesting a minimum effective daily dose. Building upon this, we administered a total dose of 540 mg/kg, composed of a loading dose of 180 mg/kg and maintenance dose of 19 mg/kg eq. Ptx (Group 7). This regimen resulted in the best results, with an initial tumor regression followed by a long-lasting tumor growth suppression (Figure 5B).

Table 1. Simulated treatment groups. For all groups, standard treatment or loading dose started 17 days after tumor inoculation and lasted for 21 days. If the group received a loading dose, *maintenance* treatment started 48 h later (i.e., 19 days after tumor inoculation) and was administered daily.

Treatment group	Total dose (mg/kg)	Loading dose (mg/kg)	Treatment dose (mg/kg)	Maintenance treatment (mg/kg)	Number of administrations
Group 1	180	-	60	-	3
Group 2	180	-	180	-	1
Group 3	180	-	8.57	-	21
Group 4	180	60	-	6.32	1+19
Group 5	300	180	-	6.32	1+19
Group 6	300	-	14.29	-	21
Group 7	540	180	-	19	1+19

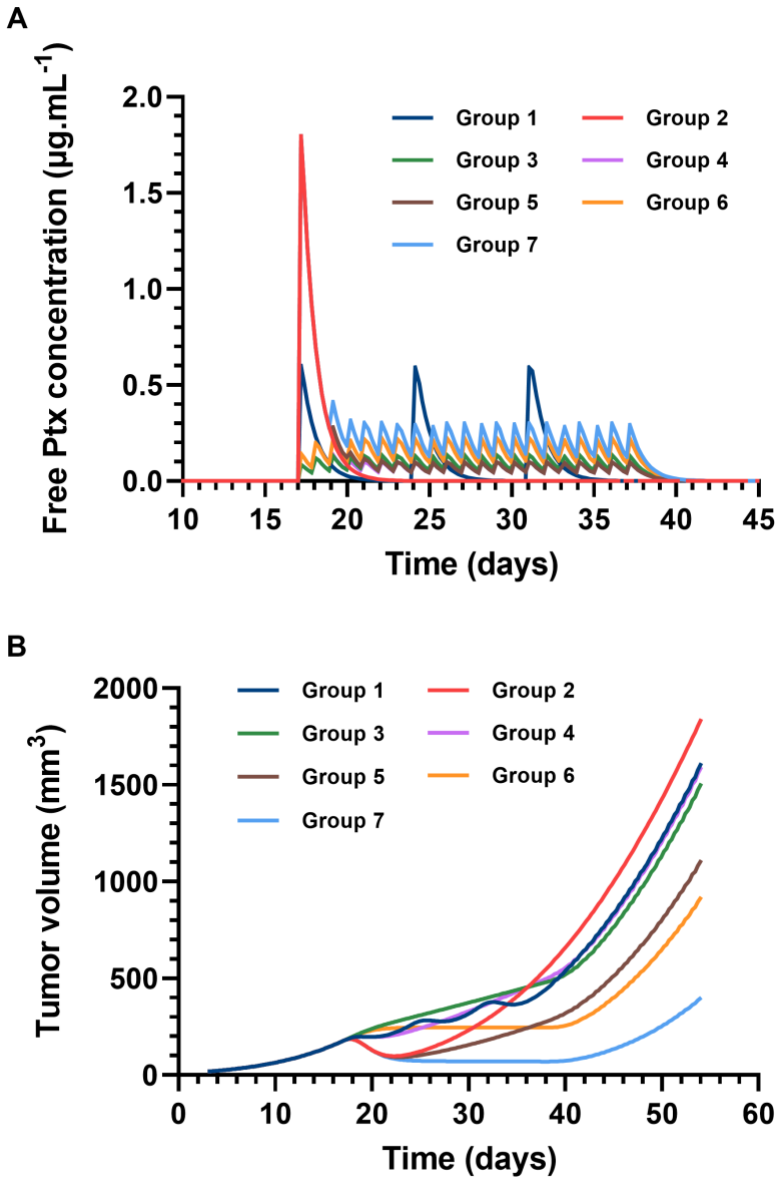

Figure 5. Pharmacokinetic and pharmacodynamic simulations. Pharmacokinetic (A) and pharmacodynamic (B) model predictions of simulated treatment Groups 1-7. The loading/initial doses for Groups 2, 5 and 7 are overlaid.

In vivo validation of dosing schedules

The 7 selected treatment groups (Table 1) were subsequently tested *in vivo* on MCF-7 tumor-bearing mice (Figure 6A-C). They exhibited significant differences in tumor size following treatment (day 52, $p < 0.0001$, one-way ANOVA). The simulation-based predictions showed remarkable agreement with the experimental observations, across all groups except for the high-dose treatments (180 mg/kg; Groups 2 and 5), which showed greater efficacy than predicted. This is likely due to possible nonlinear PK of Ptx-PAAm at this dose range. Because the Ptx-PAAm formulation does not contain

Cremophor EL (the standard Ptx excipient, known to contribute to nonlinear PK of Taxol [21]), we initially assumed a linear PK. However, these results suggest that this assumption may not hold, which could be explained by the fact that the PK model was developed at a lower dose (7 mg/kg). Drug exposure might be prolonged in the experimental data, leading to slower regrowth than simulated.

When assessing the anticancer activity of each group, at the same total dose, Group 2 outperformed Groups 1, 3 and 4, thus strengthening the interest of a high loading dose (tumor volumes at 52 days: 315 ± 269 mm^3 versus 978 ± 384 mm^3, p = 0.0036, 932 ± 458 mm^3, p = 0.0025, and 819 ± 465 mm^3, p = 0.04, respectively, Tukey's tests). Similar results were observed at higher total dose between Groups 5 (loading dose + maintenance treatment) and 6 (daily administration) with end tumor volumes of 217 ± 161 mm^3, and 630 ± 384 mm^3, respectively (p = 0.15, Tukey's test). As predicted by the model, a higher loading dose (Group 5: 180 mg/kg, vs. Group 4: 60 mg/kg) resulted in not only a stronger initial response but also a more sustained efficacy (Figure 6D). Tumor volumes after 52 days were 819 ± 465 mm^3 and 217 ± 161 mm^3, respectively, p = 0.0023, t-test and p = 0.0093, Tukey's test). Also, in line with the model predictions, increasing the maintenance dose from 6.3 mg/kg (Group 5) to 19 mg/kg (Group 7) resulted in greater and more durable efficacy, lasting up to 30 days after treatment termination (Figure 6D). The difference in tumor volumes after 52 days were substantial (217 ± 161 mm^3 vs. 31 ± 46 mm^3, respectively), although not significant when controlling for multiple hypothesis testing (p = 0.9, Tukey's test). Survival was found to be higher for all model-driven schedules (i.e., Groups 2 to 7) compared to the standard schedule (Group 1) (Figure 6B). The safety constraints accounted for in the model resulted in good treatment tolerance (no weight loss observed in any group, Figure 6C).

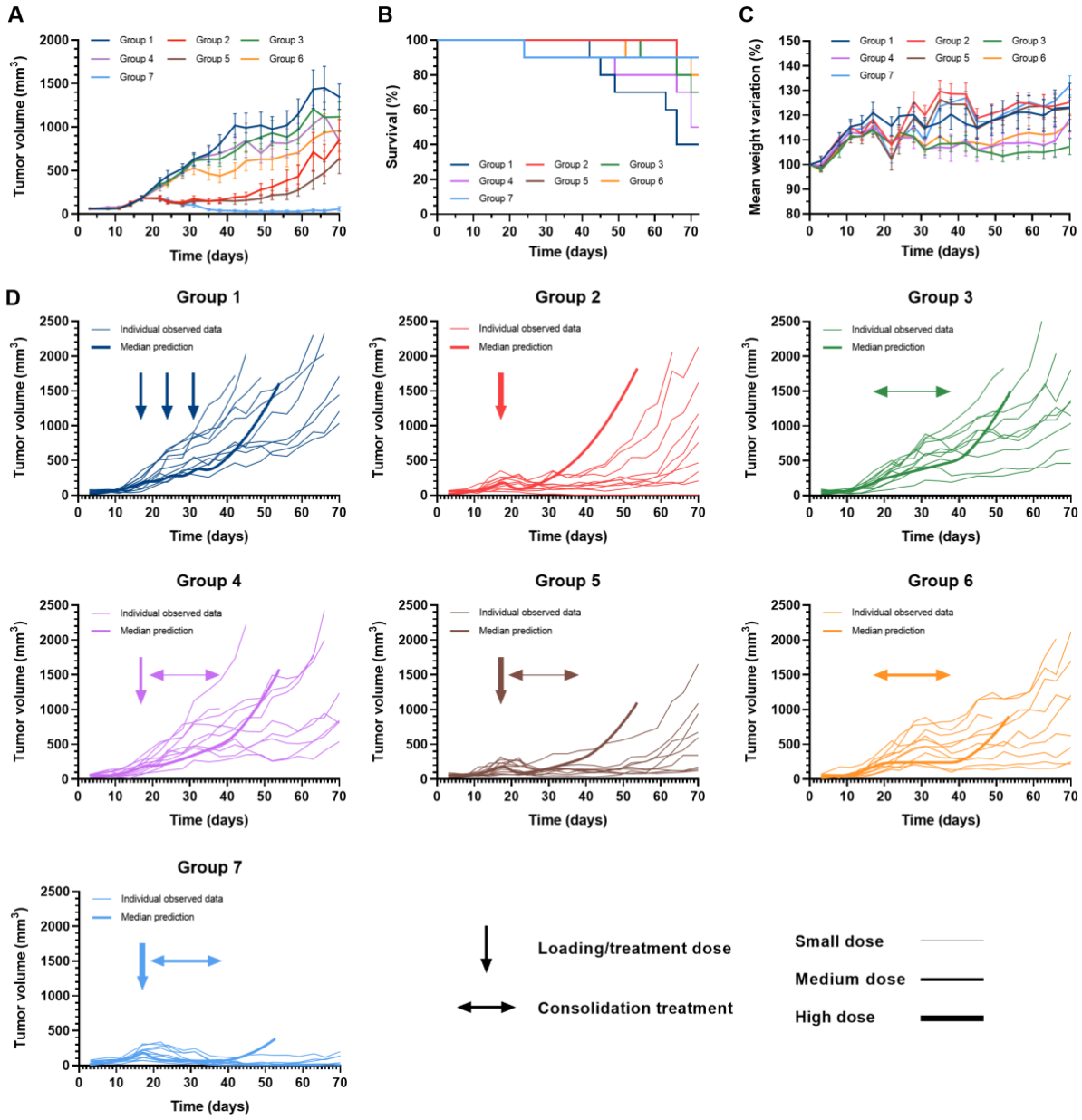

Figure 6. *In vivo* results and model validation. (A) Tumor growth (means ± SD, n = 10 per group). (B) Overall survival. Groups 5 and 7 are perfectly overlaid and meet Group 2 at the end of experiment. (C) Relative body weight change of mice as a function of time after SC Ptx-PAAm injection following specific scheduling. The values are expressed as the means ± SD (n = 10). (D) Median prediction (thick line) simulated with Simulx® software *[22]* over 54 days and individual observations (thin lines) of tumor growth for all treatment groups. The treatment groups have been schematized using arrows whose thickness is proportional to the dose with 3 levels (small, medium and high dose). Horizontal arrows represent daily administration (maintenance treatment).

DISCUSSION

In this study we demonstrated that combining *in vivo* and *in silico* modeling can successfully guide the design of optimized dosing schedules for nanocarrier-based chemotherapies, here applied to a subcutaneously administered polymer prodrug of paclitaxel (Ptx-PAAm). We developed and validated a mechanistic model of the pharmacokinetics and antitumor efficacy of SC Ptx-PAAm, trained on *in vivo* data and prospectively tested on independent datasets. Simulations revealed that a regimen combining a high loading dose followed by a daily maintenance dose achieved the highest efficacy, with a 60% complete response rate and no observed toxicity. These predictions were validated *in vivo*, confirming the model's ability to improve therapeutic outcomes over standard regimens.

A previous experimental study on water-soluble Ptx-PAAm polymer prodrugs not only showed that it could be safely administered subcutaneously, but also that the sustained release of Ptx (i.e., longer half-life, T_{max} and mean residence time associated with lower C_{max}) could lead to greater anticancer efficacy [14]. Other examples of Ptx-polymer conjugates previously developed, such as Ptx-polyglutamic acid conjugates, showed similar results after IV administration in preclinical studies [23]. However, further development was halted after failing to show an improvement in patient survival in Phase III trials [24], despite improved treatment convenience and reduced toxicities. All studies conducted to date on Ptx-polyglutamic acid conjugates have followed the traditional MTD paradigm [25], omitting the investigation of more refined schedules such as metronomic therapy [26,27]. This highlights the need for more rational, data-driven development strategies that account for the unique kinetics of these compounds.

While nanocarrier drug delivery systems have been widely studied for their potential to improve solubility, bioavailability, and tumor accumulation of chemotherapeutic agents, the optimization of their dosing regimens remains largely empirical. The majority of previous studies in the field have focused either on physicochemical design [28] or on demonstrating improved biodistribution profiles in preclinical models [9,11], without directly addressing the impact of altered PK on treatment efficacy over time. Importantly, most regimens for nanocarriers are still derived from conventional MTD-

based schedules initially developed for free drugs with rapid clearance and high systemic toxicity [25].

Mathematical modeling offers a powerful alternative to guide rational treatment design, but its application to nanocarrier systems, and especially polymer prodrugs, remains limited. Notably, prior PK/PD models in oncology have focused on free drugs [29–31] or liposomal formulations [13,32], often without validation beyond the PK profile. A recent modeling study involving gemcitabine and nab-Ptx proposed optimal schedules based on xenograft data [12], but did not prospectively validate these *in silico* predictions. To our knowledge, our study is the first to develop and prospectively validate a fully integrated PK/PD model for a nanocarrier-based chemotherapy, demonstrating its predictive power *in vivo* and its ability to inform new, more effective treatment strategies.

In addition, our work builds upon and extends earlier efforts in metronomic chemotherapy [7,26,33], and model-based optimization of anticancer regimens [8,34], by integrating mechanistic modeling with high-quality preclinical datasets and leveraging the flexibility and versatility of SC administration. Importantly, the SC route, despite its potential for improved patient comfort, cost reduction, and reduced hospital burden, has remained underexplored for vesicant chemotherapies like Ptx. The use of polymer prodrugs such as Ptx-PAAm enables this transition, and our model provides a rational framework to optimize SC regimens tailored to the altered kinetics and dynamics of such systems.

In this sense, our study makes several key contributions. It establishes a validated framework for using PK/PD modeling to design optimized schedules for polymer prodrugs, with clear experimental confirmation. The model integrates the complex kinetics of SC absorption, systemic release of free Ptx, and tumor growth inhibition, including the modeling of acquired resistance after the first administration, an aspect rarely addressed in preclinical PK/PD studies.

We also showed that the bioavailability and slower release kinetics of SC Ptx-PAAm allow for higher cumulative doses (up to 540 mg/kg eq. Ptx) without exceeding the C_{max} of IV Ptx at 7 mg/kg [14], effectively shifting the therapeutic window. This has major implications for clinical translation, especially for drugs limited by their toxicity profiles

when given intravenously. On the pharmacodynamics side, our modeling approach revealed differential efficacy between the first and subsequent administrations. This identification of drug resistance was modeled by two different E_{max} values, with $E_{max1} > E_{max2}$.

Therefore, we demonstrated that model-informed scheduling could substantially improve therapeutic outcomes. Simulation of PK profiles allowed the identification of safe dosing regimens of SC Ptx-PAAm, with higher cumulative dose. Among them, Group 7 even achieved near-complete tumor suppression and improved survival, without inducing weight loss or other observable signs of toxicity. This aligns with prior reports on the benefit of metronomic-like strategies [27,35], but also highlights the added value of a loading dose to overcome early resistance, a novel finding in the context of SC polymer prodrugs.

Lastly, our methodology can be viewed as a form of preclinical "digital twin", allowing the simulation and testing of numerous treatment strategies prior to animal experimentation. This contributes to the refinement and reduction of animal use, in line with the 3Rs principle [36,37], and represents a significant step toward the digitization of preclinical oncology.

Despite its strengths, this work has several limitations. First, the model was developed and validated in a single xenograft model (MCF-7), which, although well-established, does not reflect the full heterogeneity of breast cancers, nor of other tumor types. It also lacks immune components due to the use of immunodeficient mice. Future developments should test the generalizability of the model across tumor types and immunocompetent models [27].

Second, although we included resistance as a decrease in efficacy after the first administration, its mechanistic basis was not investigated. We hypothesize that after the first administration the most sensitive cells died more rapidly, leaving only room for the proliferation of resistant cells. Indeed, it has been recently shown in a 3D ovarian cancer *in vitro* model that there is a maximum concentration (i.e., single dose 25 nM Ptx *versus* four weekly doses 10 nM Ptx) that should not be exceeded in order to avoid the proliferation of resistant cells [35]. However, the detailed mechanistic basis of resistance was not investigated. Understanding whether this resistance arises from

pharmacological tolerance, tumor adaptation, or microenvironmental factors would help design even more robust strategies. Additionally, resistance mechanisms may differ in human tumors, limiting the extrapolation of the current findings.

Finally, the current model does not incorporate variability in tumor burden, drug exposure, or sensitivity across individuals, beyond random effects on model parameters. Incorporating patient-level covariates in future translational models could pave the way toward personalized scheduling strategies.

Nevertheless, our results provide a strong rationale for the use of model-driven strategies in the development of nanocarrier-based chemotherapies. A natural next step would be to extend this approach to other drugs, tumor types, and *in vivo* models. This would test the broader applicability of the digital twin framework and support its use in early-phase drug development pipelines.

Another perspective lies in coupling this modeling approach with toxicity prediction models or physiologically-based-PK models of organ toxicity. While it captured efficacy well, toxicity was not explicitly modeled beyond weight monitoring. Although no weight loss was observed, more sensitive markers (e.g., neurotoxicity) would allow a better characterization of the therapeutic window [38]. This would enable true efficacy-toxicity optimization and support rational design of phase I/II studies.

Furthermore, as SC administration becomes increasingly feasible for oncologic therapies [15,17], optimization of SC regimens may significantly improve the accessibility and convenience of cancer care. This aligns with broader trends in personalized medicine, where the scheduling, dosing, and route of administration are adapted to the individual patient and drug properties.

Finally, this work contributes to the growing interest in using digital twins for oncology, not only at the patient level, but also in preclinical development [39,40]. Such frameworks offer a new paradigm for reducing costs, accelerating timelines, and improving success rates of translational research in oncology.

CONCLUSION

In this work, we have developed a PK/PD model that covers a wide range of therapeutic regimens of a recently-developed subcutaneously-administered water-soluble polymer prodrug for cancer therapy, chosen as a nanocarrier drug delivery system proof-of-concept and, most importantly, that allows prediction of its *in vivo* performances and thus optimization of its anticancer efficacy. Among the different administration schedules, a loading dose of 180 mg/kg followed 48 h later by daily administration of 19 mg/kg for 19 days was found to be the most efficient one, with a complete response of 60% in breast cancer bearing mice.

To the best of our knowledge, this work represents the first example of experimental PK/PD model for nanocarrier drug delivery systems whose predictions of anticancer efficacy are validated *in vivo*. This approach could save a lot of time, reduce costs and, above all, considerably reduce animal experimentation by efficiently refining the administration scheme, which is of key importance in the context of the 3Rs principles (Replacement, Reduction and Refinement).

Importantly, this work provides strong evidence that this PK/PD model could be used as an accurate, forward-looking tool for predicting and optimizing the therapeutic efficacy of nanocarrier drug delivery systems administered via the SC route, which is receiving increasing attention in the field of nanomedicine.

MATERIALS AND METHODS

Materials

Azobisisobutyronitrile (98%, AIBN) was purchased from Sigma-Aldrich and recrystallized from ethanol. Acrylamide (> 99%, AAm) was purchased from Sigma-Aldrich and recrystallized from chloroform. Cyano-4-[(dodecylsulfanylthiocarbonyl) sulfanyl]pentanoic acid (97%, CDSPA), 1-(3-dimethylaminopropyl)-3-ethylcarbodiimide hydrochloride (> 97%, EDC.HCl) and 4-dimethylaminopyridine (98%, DMAP) were purchased from Sigma-Aldrich and used as received. Paclitaxel (Ptx) was purchased from Carbosynth. Deuterated DMSO (DMSO-d_6) was obtained from Eurisotop. Anhydrous dichloromethane (DCM) was purchased from Sigma-Aldrich.

Analytical methods

Nuclear magnetic resonance (NMR) spectroscopy

NMR spectroscopy was performed in 5 mm diameter tubes in DMSO-d_6 at 25 °C. ^{1}H-NMR spectroscopy was performed on a Bruker Avance 300 spectrometer at 300 MHz and on a Bruker Avance 400 at 400 MHz. The chemical shift scale was calibrated based on the internal solvent signals (δ = 2.50 ppm for DMSO-d_6). ^{13}C-NMR spectroscopy was performed on a Bruker Avance 400 at 100 MHz. Data were processed with MestReNova 14.0.0 software.

Size exclusion chromatography (SEC)

SEC was performed at 60 °C using two columns in series from Agilent Technologies (PL PolarGel-M, 300 × 7.5 mm; bead diameter 8 µm; molar mass range 1 000–500 000 g.mol^{-1}) preceded by a guard column from Agilent Technologies (PL PolarGel-M, 7.5 × 50 mm; bead diameter 8 µm) and a triple detection system (Viscotek TDA/GPCmax from Malvern) with a differential refractive index detector, low and right-angle light scattering detectors and a differential viscometer detector. The eluent was DMSO with 100 mM lithium bromide (LiBr) and 0.4 wt % of 2,6-di-*tert*-butyl-4-methylphenol (BHT) as a flowrate marker at a flow rate of 0.7 mL min^{-1}. The system was calibrated using pullulan standards (peak molar masses, M_p = 180–1 450 000

g.mol^{-1}) from Agilent Technologies. This allowed the determination of the number-average molar mass (M_n), the weight-average molar mass (M_w) and the dispersity ($Đ = M_w/M_n$). All samples were filtered over 0.22 µm Nylon filters prior to injection. Data was collected and processed with OmniSEC 4.0 software.

Mass spectrometry

Mass spectra were recorded with a Bruker Esquire-LC instrument. High-resolution mass spectra (ESI) were recorded on an ESI/TOF (LCT, Waters) LC-spectrometer.

Synthesis procedures

Synthesis of Ptx-CDSPA RAFT agent

In a 25 mL round-bottom flask, CDSPA 1.17 mmol, 0.472 g), DMAP (1.46 mmol, 0.168 g) and EDC.HCl (1.46 mmol, 0.280 g) were dissolved in anhydrous dichloromethane (2.5 mL). The mixture was sonicated in an ultrasonic bath for 15 min. A solution of Ptx 1.17 mmol, 0.999 g) in DCM (2 mL) was added dropwise at 0 °C. The reaction mixture was stirred for another 22 h at room temperature. 30 mL ethyl acetate (EtOAc) was added into the flask and the reaction medium was then transferred into a separating funnel, from which the product was extracted by 2 x 30 mL $NaHCO_3$ aqueous solution. The organic phase was dried over $MgSO_4$. The residue was purified by flash chromatography (SiO_2, from DCM/EtOAc = 10/1 to DCM/EtOAc = 2/3, v/v). 0.667 g 0.538 mmol) of Ptx-CDSP was obtained as yellow powder. Yield = 46 %

^{1}H NMR (400 MHz, DMSO): δ (ppm): 8.86 (d, 1H), 7.99–7.86 (p, 4H), 7.73–7.34 (m, 10H), 7.21 (m, 1H), 6.28 (s, 1H), 6.12 (d, 1H), 5.89 (t, 1H), 5.40 (t, 2H), 4.88 (t, 2H), 4.67 (s, 1H), 4.58 (t, 1H), 4.14–3.97 (m, 3H), 3.61 (d, 1H), 2.22 (s, 3H), 2.10 (s, 3H), 1.78 (s, 3H), 1.50 (s, 3H), 1.01 (s, 6H).

^{13}C NMR (75 MHz, $CDCl_3$): δ (ppm): 216.82, 203.72, 171.13, 170.67, 169.80, 167.88, 167.01, 142.58, 136.78, 133.64, 133.51, 132.92, 132.03, 130.22, 129.23, 129.16, 128.72, 128.58, 127.14, 126.52, 84.44, 81.09, 79.14, 76.42, 75.58, 75.14, 74.65, 72.10, 72.01, 58.53, 52.80, 46.28, 45.62, 43.18, 39.24, 37.13, 35.55, 33.62, 31.88, 29.59, 29.52, 29.39, 29.30, 29.04, 28.91, 27.65, 26.81, 24.80, 24.74, 22.71, 22.66, 22.09, 20.78, 14.79, 14.09, 9.60.

High-resolution mass spectrometry (ESI^+): *m/z* = $[M+H^+]$. Calculation = 1238.4877, found = 1239.4950.

Synthesis of Ptx-PAAm

Ptx-PAAm polymer prodrugs were synthesized by the "*drug initiated*" method from Ptx-CDSPA as a RAFT agent, as published elsewhere, with some modifications [41]. AIBN 0.0107 mmol, 1.75 mg) , Ptx-CDSPA (0.0533 mmol, 66.1 mg), AAm (0.018 mol, 1.303 g) and DMSO (10 mL) were added in a 25 ml glass vial which was with argon ballon to bubble the solvent. After 20 minutes, the vial was immersed into a 70 °C-preheated oil bath. After 24 h stirring, the crude product was precipitated three times in cold methanol. Then the polymer was solubilized in deionized water and left in a 2 KDa Spectra/por 1 dialysis bag for dialysis for 3 days to remove unreacted monomers. The dialysis water was changed twice per day. Then the content of the dialysis bag was freeze-dried to give the Ptx-PAAm polymer prodrug as a white and spongy solid. The synthesis was repeated 19 times in a reproducible manner, to achieve a sufficient quantity for the efficacy study. $M_{n,SEC\ (pullulan\ std.)}$ = 23050 ± 1530 g/mol^{-1}, $Đ$ = 1.15 ± 0.05, total mass = 21.1 g (n = 19).

Data for model development

All data used to build the model come from previously published work, resulting from *in vivo* comparative studies between SC Ptx-PAAm (labelled P3e for Ptx-*ester*-4-cyano-4-[(dodecylsulfanylthiocarbonyl)sulfanyl]pentanoic acid) and IV Ptx (i.e., Taxol) [41]. PK and efficacy studies were conducted according to the European rules (86/609/EEC and 2010/ 63/EU) and the Principles of Laboratory Animal Care and legislation in force in France (Decree No. 2013-118 as of February 1, 2013) and obtained experimental approval from the Ethical Committee C2EA-26 (Comité d'éthique en expérimentation animale de l'IRCIV, Authorization number APAFIS#7756) and the Institutional Animal Care and Use Committee of Oncodesign (Oncomet) approved by French authorities (CNREEA agreement N° 91), respectively. Briefly, for the PK study, two treatment groups of IV Ptx and SC Ptx-PAAm at 7mg/kg eq. Ptx were administered to 72 seven-week-old female BALB/c OlaHsd mice (~22 g; Envigo, France) and blood was collected at 0.25, 0.5, 1, 2, 4, 7, 24, 48, and 72 h and analyzed by LC-MS/MS. PK values below the limit of quantification (0,005 µg/mL) were

considered as censored observations. For the efficacy study, 52 six- to eight-week-old female BALB/c nude mice were inoculated with 10×10^6 MCF-7 cells. Q7Dx3 treatment began 17 days after inoculation and was administered as follows: (i) SC PAAm at 1520 mg/kg (negative control); (ii) SC Ptx-PAAm at 15 mg/kg (eq. Ptx); (iii) SC Ptx-PAAm at 60 mg/kg (eq. Ptx); and (iv) IV Ptx at 15 mg/kg. Tumor volume was measured twice weekly with a caliper and estimated using the following formula: volume = (length × width^2)/2.

Pharmacokinetic modeling

A PK model including administration as IV Ptx or SC Ptx-PAAm at 7 mg/kg eq. Ptx was developed using the nonlinear mixed-effects modeling statistical framework [42].

One-, two-, and three-compartment models with linear or mixed elimination were tested for Ptx-PAAm [29–31]. The absorption phase was modeled using first-order absorption rates with or without a lag time. All equations are given in Table S3. For all models, we set the time of administration t_0= 0 and the amount of Ptx in the main compartment A_0= 0. A proportional error best described the data. Because the *in vivo* data came from a non-longitudinal study (i.e., animals were sacrificed at each time point), we could not distinguish the intra-individual error from the residual error. Therefore, the standard deviation of the proportional error model was manually tested and set to 10%. Apparent bioavailability of SC Ptx-PAAm (F_t) was first implemented in the model as a free parameter following a logit normal distribution and subsequently fixed to its estimated value (36%).

Pharmacodynamic modeling

Multiple pharmacodynamic models were tested against the data for the following processes (see Table S3):

(i) Untreated tumor growth for which several models were tested and calibrated with the negative control data (i.e., PAAm 60 mg/kg eq.): Exponential, Power Law, Logistic, Gompertz and Reduced Gompertz models [20]. For all models, the number of tumor cells inoculated at time t_0= 0 was 10^7. Therefore we fixed

the initial volume TV_0 = 10 mm^3 in the whole dataset [43]. We set t_0 and TV_0 as initial conditions of the equations.

(ii) Effect of Ptx on cancer cells for which several models were simultaneously tested and calibrated using PD data (i.e., PAAm 60 mg/kg eq. acting as control , IV Ptx 15 mg/kg and SC Ptx-PAAm 15 mg/kg eq. Ptx): Simeoni, Norton Simon, Log Kill and threshold killing models.

(iii) Resistance to Ptx.

The error model was described using the Combined 2 function from Monolix® software [44], where $y = f + \sqrt{a^2 + b^2(f^c)^2}\varepsilon$. The function g is a combination of a constant term and a term proportional to the structural model $f(g = bf^c)$, and the additional parameters are ξ=(a,b) and c is fixed at 1.

Mixed-effects statistical modeling

Denoting by M a (PK or PD) structural model, longitudinal observations y_j^i at time t_j^i in animal i with parameters θ^i were assumed to follow the observation model:

$$y_j^i = M(t_j^i; \theta^i) + \varepsilon_j^i,$$

where $\varepsilon_j^i \sim \mathcal{N}(0, \sigma_j^i)$ is a Gaussian-distributed error model. Its structure was tested between additive ($\sigma_j^i = a, \forall i, j$), proportional ($\sigma_j^i = bM(t_j^i)$) and combined ($\sigma_j^i = a + bM(t_j^i)$). To describe inter-animal variability, some individual parameters θ^i were assumed to follow log-normal distributions:

$$\ln(\theta^i) = \ln(\theta_{pop}) + \eta^i, \qquad \eta^i \sim \mathcal{N}(0, \omega^2)$$

with population-level parameters θ_{pop} and ω. The other individual parameters were assumed constant in the population (no random effects, see Table S1). Estimation of these was performed using the stochastic approximation of expectation maximization algorithm implemented in the Monolix software [44,45].

PK/PD model validation

Model selection was based on goodness-of-fit numerical criteria such as values of the OFV (i.e., -2 log likelihood) for nested models or, alternatively, the Akaike information

criteria (AIC), alternatively. Graphical criteria such as Visual Predictive Checks (VPC), individual fits and observations *versus* population or individual predictions were also used. In addition, parametric identifiability was assessed using relative standard errors (RSE) computed from the Fisher information matrix by the Monolix® software [44]. RSEs were considered acceptable if under 30% or 50% for θ_{pop} (fixed effects) and ω (random effects), respectively. Robustness of the convergence was assessed using sensitivity test on all initial parameters of the model.

The PK/PD model was calibrated using the PAAm acting as control (60 mg/kg eq.), IV Ptx (15 mg/kg) and SC Ptx-PAAm (15 mg/kg eq. Ptx) treatment groups (i.e., training data set). It was then evaluated for its ability to predict the SC Ptx-PAAm 60 mg/kg (eq. Ptx) group (i.e., test data set).

In silico scheduling exploration

Both training and test data sets were implemented on the final PK/PD model for scheduling exploration. Multiple dosing regimens were explored using the Simulx software [22]. Concentrations and tumor growth were simulated in 10 animals weighing 22 grams each. The simulated treatment regimens are described in Table 1. Briefly, different total dose regimens were simulated for SC Ptx-PAAm (180 mg/kg, 300 mg/kg and 540 mg/kg Ptx eq.), administered once, weekly, or daily, for 21 days, starting 17 days after tumor inoculation. In addition, we tested the effect of a loading dose of 60 mg/kg Ptx or 180 mg/kg Ptx eq., (previously determined as the MTD [41]), followed by a 48 hour washout period prior to daily administrations. Simulations were performed for 54 days.

In vivo scheduling validation

All the above simulated treatment groups (Table 1) were further tested *in vivo*.

Ethical Protocol

Animal housing and experimental procedures *were* conducted according to the French and European Regulations and the National Research Council Guide for the Care and Use of Laboratory Animals. The animal facility *was* authorized by the French authorities (Dijon: Agreement N° C 21 231 011 EA). All animal procedures (including surgery, anesthesia and euthanasia as applicable) used in the current study

(230454/ACT1 MCF-7 SC/Ethical protocol: 2022-03 ONCO SC) *were validates by* the Institutional Animal Care and Use Committee of Oncodesign Services (Oncomet) approved by French authorities [CNREEA agreement N° 91 (Oncodesign Services)].

Efficacy study

The study was performed on 70 Balb/c Nude mice of 6-8 weeks at reception. 10^7 human breast cancer cells in 200 µL of RPMI 1640 medium (i.e., MCF-7) were inoculated into the right flank of the mice, 24-72H after a whole-body irradiation with a gamma-source (2 Gy (Nude mice), 60Co, BioMep, France). 17 days after tumor inoculation, the mice were randomly divided into seven treatment groups of ten mice each, all receiving SC Ptx-PAAm (Table 1). Tumor volume measurements were performed twice a week, using caliper and the following formula: $Volume = \frac{(length\,.\,width^2)}{2}$ and compared for treatment efficacy on Day 52, using analysis of variance (ANOVA) with multiple comparison (Tukey's test). Animal well-being was checked daily, and when Humane Endpoint was reached, mice were euthanized by overdose of gas anesthesia (isoflurane) followed by cervical dislocation.

ACKNOWLEDGEMENTS

This project has received funding from the European Research Council (ERC) under the European Union's Horizon 2020 research and innovation program (Grant agreement No. 771829).

AUTHOR CONTRIBUTIONS

J.N conceived the project and obtained funding. S.B and J.N designed the study. A.R, R.L and S.M carried out the simulations. J.C. synthesized the polymer prodrugs. J.N, S.B, A.R, R.L and S.M contributed to the interpretation of the results. A.R took the lead in writing the paper with close supervision from S.B and J.N and input from all the authors.

COMPETING INTEREST

The authors declare no competing interest.

REFERENCES

1. Chen S, Cao Z, Prettner K, Kuhn M, Yang J, Jiao L, et al. Estimates and Projections of the Global Economic Cost of 29 Cancers in 204 Countries and Territories From 2020 to 2050. JAMA Oncol. 2023;9: 465–472. doi:10.1001/jamaoncol.2022.7826

2. World Cancer Report 2014 - Stewart B. W.; Wild C. P.: 9789283204299 - AbeBooks. [cited 5 May 2025]. Available: https://www.abebooks.fr/9789283204299/World-Cancer-Report-2014-Stewart-9283204298/plp

3. Koh DBC, Gowardman JR, Rickard CM, Robertson IK, Brown A. Prospective study of peripheral arterial catheter infection and comparison with concurrently sited central venous catheters. Crit Care Med. 2008;36: 397–402. doi:10.1097/CCM.0b013e318161f74b

4. Guerassimoff L, Ferrere M, Bossion A, Nicolas J. Stimuli-sensitive polymer prodrug nanocarriers by reversible-deactivation radical polymerization. Chem Soc Rev. 2024;53: 6511–6567. doi:10.1039/D2CS01060G

5. Mitchell MJ, Billingsley MM, Haley RM, Wechsler ME, Peppas NA, Langer R. Engineering precision nanoparticles for drug delivery. Nat Rev Drug Discov. 2021;20: 101–124. doi:10.1038/s41573-020-0090-8

6. Ekladious I, Colson YL, Grinstaff MW. Polymer–drug conjugate therapeutics: advances, insights and prospects. Nat Rev Drug Discov. 2019;18: 273–294. doi:10.1038/s41573-018-0005-0

7. Benzekry S, Pasquier E, Barbolosi D, Lacarelle B, Barlési F, André N, et al. Metronomic reloaded: Theoretical models bringing chemotherapy into the era of precision medicine. Semin Cancer Biol. 2015;35: 53–61. doi:10.1016/j.semcancer.2015.09.002

8. Bonate PL. Pharmacokinetic-Pharmacodynamic Modeling and Simulation. 2nd ed. 2011. New York: Springer-Verlag New York Inc.; 2011.

9. Lindqvist A, Fridén M, Hammarlund-Udenaes M. Pharmacokinetic considerations of nanodelivery to the brain: Using modeling and simulations to predict the outcome of liposomal formulations. European Journal of Pharmaceutical Sciences. 2016;92: 173–182. doi:10.1016/j.ejps.2016.07.003

10. Vaghi C, Fanciullino R, Benzekry S, Poignard C. Macro-scale models for fluid flow in tumour tissues: impact of microstructure properties. J Math Biol. 2022;84: 27. doi:10.1007/s00285-022-01719-1

11. Vasalou C, Harding J, Jones RDO, Hariparsad N, McGinnity DF. Interspecies evaluation of a physiologically based pharmacokinetic model to predict the biodistribution dynamics of dendritic nanoparticles. PLoS One. 2023;18: e0285798. doi:10.1371/journal.pone.0285798

12. Kobuchi S, Morita A, Jonan S, Amagase K, Ito Y. Translational PK-PD/TD modeling of antitumor effects and peripheral neuropathy in gemcitabine and nab-paclitaxel chemotherapy from xenograft mice to patients for optimal dose and schedule. Cancer Chemother Pharmacol. 2024;93: 365–379. doi:10.1007/s00280-023-04625-5

13. Luo D, Carter KA, Molins EAG, Straubinger NL, Geng J, Shao S, et al. Pharmacokinetics and pharmacodynamics of liposomal chemophototherapy with short drug-light intervals. Journal of Controlled Release. 2019;297: 39–47. doi:10.1016/j.jconrel.2019.01.030

14. Bordat A, Boissenot T, Ibrahim N, Ferrere M, Levêque M, Potiron L, et al. A Polymer Prodrug Strategy to Switch from Intravenous to Subcutaneous Cancer Therapy for Irritant/Vesicant Drugs. J Am Chem Soc. 2022;144: 18844–18860. doi:10.1021/jacs.2c04944

15. Anderson KC, Landgren O, Arend RC, Chou J, Jacobs IA. Humanistic and Economic Impact of Subcutaneous Versus Intravenous Administration of Oncology Biologics. Future Oncol. 2019;15: 3267–3281. doi:10.2217/fon-2019-0368

16. Stoner KL, Harder H, Fallowfield LJ, Jenkins VA. Intravenous versus Subcutaneous Drug Administration. Which Do Patients Prefer? A Systematic Review. Patient. 2014. doi:10.1007/s40271-014-0075-y

17. Tomasini L, Ferrere M, Nicolas J. Subcutaneous drug delivery from nanoscale systems. Nat Rev Bioeng. 2024;2: 501–520. doi:10.1038/s44222-024-00161-w

18. Gradishar WJ. Taxanes for the treatment of metastatic breast cancer. Breast Cancer (Auckl). 2012;6: 159–171. doi:10.4137/BCBCR.S8205

19. Simeoni M, Magni P, Cammia C, De Nicolao G, Croci V, Pesenti E, et al. Predictive pharmacokinetic-pharmacodynamic modeling of tumor growth kinetics in xenograft models after administration of anticancer agents. Cancer Res. 2004;64: 1094–1101. doi:10.1158/0008-5472.can-03-2524

20. Vaghi C, Rodallec A, Fanciullino R, Ciccolini J, Mochel JP, Mastri M, et al. Population modeling of tumor growth curves and the reduced Gompertz model improve prediction of the age of experimental tumors. PLoS Comput Biol. 2020;16: e1007178. doi:10.1371/journal.pcbi.1007178

21. Sparreboom A, van Zuylen L, Brouwer E, Loos WJ, de Bruijn P, Gelderblom H, et al. Cremophor EL-mediated alteration of paclitaxel distribution in human blood: clinical pharmacokinetic implications. Cancer Res. 1999;59: 1454–1457.

22. Simulx® software version 2023R1 (Lixoft-Simulations Plus, Antony, France, http://lixoft.com/),.

23. Singer JW. Paclitaxel poliglumex (XYOTAX™, CT-2103): A macromolecular taxane. Journal of Controlled Release. 2005;109: 120–126. doi:10.1016/j.jconrel.2005.09.033

24. Langer CJ, O'Byrne KJ, Socinski MA, Mikhailov SM, Leśniewski-Kmak K, Smakal M, et al. Phase III trial comparing paclitaxel poliglumex (CT-2103, PPX) in combination with carboplatin versus standard paclitaxel and carboplatin in the treatment of PS 2 patients with chemotherapy-naïve advanced non-small cell lung cancer. J Thorac Oncol. 2008;3: 623–630. doi:10.1097/JTO.0b013e3181753b4b

25. Zhao J, Koay EJ, Li T, Wen X, Li C. A hindsight reflection on the clinical studies of poly(l-glutamic acid)-paclitaxel. Wiley Interdiscip Rev Nanomed Nanobiotechnol. 2018;10: e1497. doi:10.1002/wnan.1497

26. Pasquier E, Kavallaris M, André N. Metronomic chemotherapy: new rationale for new directions. Nat Rev Clin Oncol. 2010;7: 455–465. doi:10.1038/nrclinonc.2010.82

27. Muñoz R, Girotti A, Hileeto D, Arias FJ. Metronomic Anti-Cancer Therapy: A Multimodal Therapy Governed by the Tumor Microenvironment. Cancers. 2021;13: 5414. doi:10.3390/cancers13215414

28. Gao P, Ha-Duong T, Nicolas J. Coarse-Grained Model-Assisted Design of Polymer Prodrug Nanoparticles with Enhanced Cytotoxicity: A Combined Theoretical and Experimental Study. Angew Chem Int Ed Engl. 2024;63: e202316056. doi:10.1002/anie.202316056

29. Henningsson A, Sparreboom A, Sandström M, Freijs A, Larsson R, Bergh J, et al. Population pharmacokinetic modelling of unbound and total plasma concentrations of paclitaxel in cancer patients. European Journal of Cancer. 2003;39: 1105–1114. doi:10.1016/S0959-8049(03)00126-6

30. Callies S, de Alwis DP, Harris A, Vasey P, Beijnen JH, Schellens JH, et al. A population pharmacokinetic model for paclitaxel in the presence of a novel P-gp modulator, Zosuquidar Trihydrochloride (LY335979). Br J Clin Pharmacol. 2003;56: 46–56. doi:10.1046/j.1365-2125.2003.01826.x

31. He J, Jackson CGCA, Deva S, Hung T, Clarke K, Segelov E, et al. Population pharmacokinetics for oral paclitaxel in patients with advanced/metastatic solid tumors. CPT Pharmacometrics Syst Pharmacol. 2022;11: 867–879. doi:10.1002/psp4.12799

32. Vaghi C, Rodallec A, Ciccolini J, Fanciullino R, Benzekry S. Pharmacokinetic-pharmacodynamic modeling of antibody nanoconjugates in breast cancer treatment. preprint hal-04937059v1. 2025. Available: https://inria.hal.science/hal-04937059

33. Panthi VK, Dua K, Singh SK, Gupta G, Hansbro PM, Paudel KR. Nanoformulations-Based Metronomic Chemotherapy: Mechanism, Challenges, Recent Advances, and Future Perspectives. Pharmaceutics. 2023;15: 1192. doi:10.3390/pharmaceutics15041192

34. Iliadis A, Barbolosi D. Optimizing drug regimens in cancer chemotherapy by an efficacy-toxicity mathematical model. Comput Biomed Res. 2000;33: 211–226. doi:10.1006/cbmr.2000.1540

35. Mejia Peña C, Skipper TA, Hsu J, Schechter I, Ghosh D, Dawson MR. Metronomic and single high-dose paclitaxel treatments produce distinct heterogenous chemoresistant cancer cell populations. Sci Rep. 2023;13: 19232. doi:10.1038/s41598-023-46055-6

36. Gangwal A, Lavecchia A. Artificial intelligence in preclinical research: enhancing digital twins and organ-on-chip to reduce animal testing. Drug Discovery Today. 2025;30: 104360. doi:10.1016/j.drudis.2025.104360

37. Russell WMS. The Progress of Humane Experimental Technique. Altern Lab Anim. 2000;28: 915–922. doi:10.1177/026119290002800403

38. Cavaletti G, Alberti P, Canta A, Carozzi V, Cherchi L, Chiorazzi A, et al. Translation of paclitaxel-induced peripheral neurotoxicity from mice to patients: the importance of model selection. Pain. 2024;165: 2482–2493. doi:10.1097/j.pain.0000000000003268

39. Hernandez-Boussard T, Macklin P, Greenspan EJ, Gryshuk AL, Stahlberg E, Syeda-Mahmood T, et al. Digital twins for predictive oncology will be a paradigm shift for precision cancer care. Nat Med. 2021;27: 2065–2066. doi:10.1038/s41591-021-01558-5

40. Laubenbacher R, Mehrad B, Shmulevich I, Trayanova N. Digital twins in medicine. Nat Comput Sci. 2024;4: 184–191. doi:10.1038/s43588-024-00607-6

41. Bordat A, Boissenot T, Ibrahim N, Ferrere M, Levêque M, Denis S, et al. A Polymer Prodrug Strategy to Switch from Intravenous to Subcutaneous Cancer Therapy for Irritant/Vesicant Drugs. 2021 [cited 9 May 2022]. doi:10.26434/chemrxiv-2021-h0cwv-v2 (J. Am. Chem. Soc. article under revision)

42. Lavielle M. Mixed Effects Models for the Population Approach: Models, Tasks, Methods and Tools. CRC Press; 2014.

43. Benzekry S, Lamont C, Beheshti A, Tracz A, Ebos JML, Hlatky L, et al. Classical mathematical models for description and prediction of experimental tumor growth. PLoS Comput Biol. 2014;10: e1003800. doi:10.1371/journal.pcbi.1003800

44. Monolix® software version 2023R1 (Lixoft-Simulations Plus, Antony, France, http://lixoft.com/),.

45. Delyon B, Lavielle M, Moulines E. Convergence of a stochastic approximation version of the EM algorithm. Ann Statist. 1999;27: 94–128. doi:10.1214/aos/1018031103

46. J Bertrand, F Mentré. Mathematical expressions of the pharmacokinetic and pharmacodynamic models implemented in the Monolix software. Paris Diderot University, 2008. Lixoft.com.

47. Collins VP, Loeffler RK, Tivey H. Observations on growth rates of human tumors. Am J Roentgenol Radium Ther Nucl Med. 1956;76: 988–1000.

48. Dethlefsen LA, Prewitt JM, Mendelsohn ML. Analysis of tumor growth curves. J Natl Cancer Inst. 1968;40: 389–405. doi:10.1093/jnci/40.2.389

49. [Verhulst, 1838] Verhulst, P.-F. (1838). Notice sur la loi que la population suit dans son accroisse ment. Correspondance Mathématique et Physique, 10:113–121.

50. Winsor CP. The Gompertz Curve as a Growth Curve. Proc Natl Acad Sci U S A. 1932;18: 1–8.

51. Norton L, Simon R. Tumor size, sensitivity to therapy, and design of treatment schedules. Cancer Treat Rep. 1977;61: 1307–1317.

52. Skipper HE, Schabel FM, Wilcox WS. EXPERIMENTAL EVALUATION OF POTENTIAL ANTICANCER AGENTS. XIII. ON THE CRITERIA AND KINETICS ASSOCIATED WITH “CURABILITY” OF EXPERIMENTAL LEUKEMIA. Cancer Chemother Rep. 1964;35: 1–111.

SUPPLEMENTARY DATA

Equation S1. PK/PD Model. C = free concentration of paclitaxel (µg/mL), A = amount of Ptx (µg), V = volume of distribution (mL), k_b = absorption rate constant, k_{xy} = distribution rate constant from compartment x to compartment y and k_e = elimination rate. TV = tumor volume (mm^3), G(TV) = growth term (reduced Gompertz), γ = population-level reduced-Gompertz parameter *[20]*, TV_0 = initial tumor volume, β = individual Gompertz parameter of exponential decrease of the specific growth rate (day-1), E = Ptx potency, limited to a sigmoid maximal effect (i.e., E_{max}), larger at the first administration (i.e., $Emax1$) and k_{tran} = first-order rate constant of transit between damaged cells compartments TV_i.

Pharmacokinetics

$$\frac{dA_{ab}}{dt} = -k_b.A_{ab}$$

$$\frac{dA_1}{dt} = k_b.A_{ab} - k_e.A_1 - k_{12}.A_1 + k_{21}.A_2$$

$$\frac{dA_2}{dt} = k_{12}.A_1 - k_{21}.A_2$$

$$C = \frac{A_1}{V}$$

Pharmacodynamics

$$G(TV) = (\beta.\gamma) - \beta.\log\left(\frac{TV}{TV_0}\right).\mathrm{TV}$$

$$\frac{dTV}{dt} = G(TV) - E(C).TV$$

$$\frac{dTV_1}{dt} = E.TV - ktran.TV_1$$

$$\frac{dTV_2}{dt} = ktran.(TV_1 - TV_2)$$

$$\frac{dTV_3}{dt} = ktran.(TV_2 - TV_3)$$

$$TV = TV + TV_1 + TV_2 + TV_3$$

If treatment cure = 1:

$$E(C) = \frac{(Emax1.C)}{(EC50 + C)}$$

Else:

$$E(C) = \frac{(Emax2.C)}{(EC50 + C)}$$

Table S1. Final PK and PD parameter estimates for IV Ptx and SC Ptx-PAAm implementing the PD training data set only (i.e., SC PAAm acting 60 mg/kg eq. as control, IV Ptx 15 mg/kg and SC Ptx-PAAm 15 mg/kg). RSE (Relative standard error) is a measure of the precision of the parameter estimates, expressed as coefficient of variation (CV%); Ω is the standard deviation estimated to describe inter-animal variability using Monolix® software.

PARAMETER	ESTIMATE	RSE %
FIXED EFFECT		
V1 (mL)	10.73	5.82
K_{12} (h^{-1})	0.65	12.8
K_{21} (h^{-1})	0.51	0.0852
K_e (h^{-1})	2.76	0.134
K_b (h^{-1})	0.047	13.5
γ	7.17	5.25
β (h^{-1})	0.0013	10.3
Ktran (h^{-1})	0.05	0.681
E_{max1}(h^{-1})	6.85	59.9
E_{max2} (h^{-1})	2.51	0.753
EC50 (µg/mL)	156.1	1.22
STANDARD DEVIATION OF THE RANDOM EFFECT		
ΩV1	0.26	19.4
ΩK_{12}	0.21	37
ΩK_b	0.57	19.9
Ωβ	0.14	24.5
ΩE_{max1}	1.54	41.3

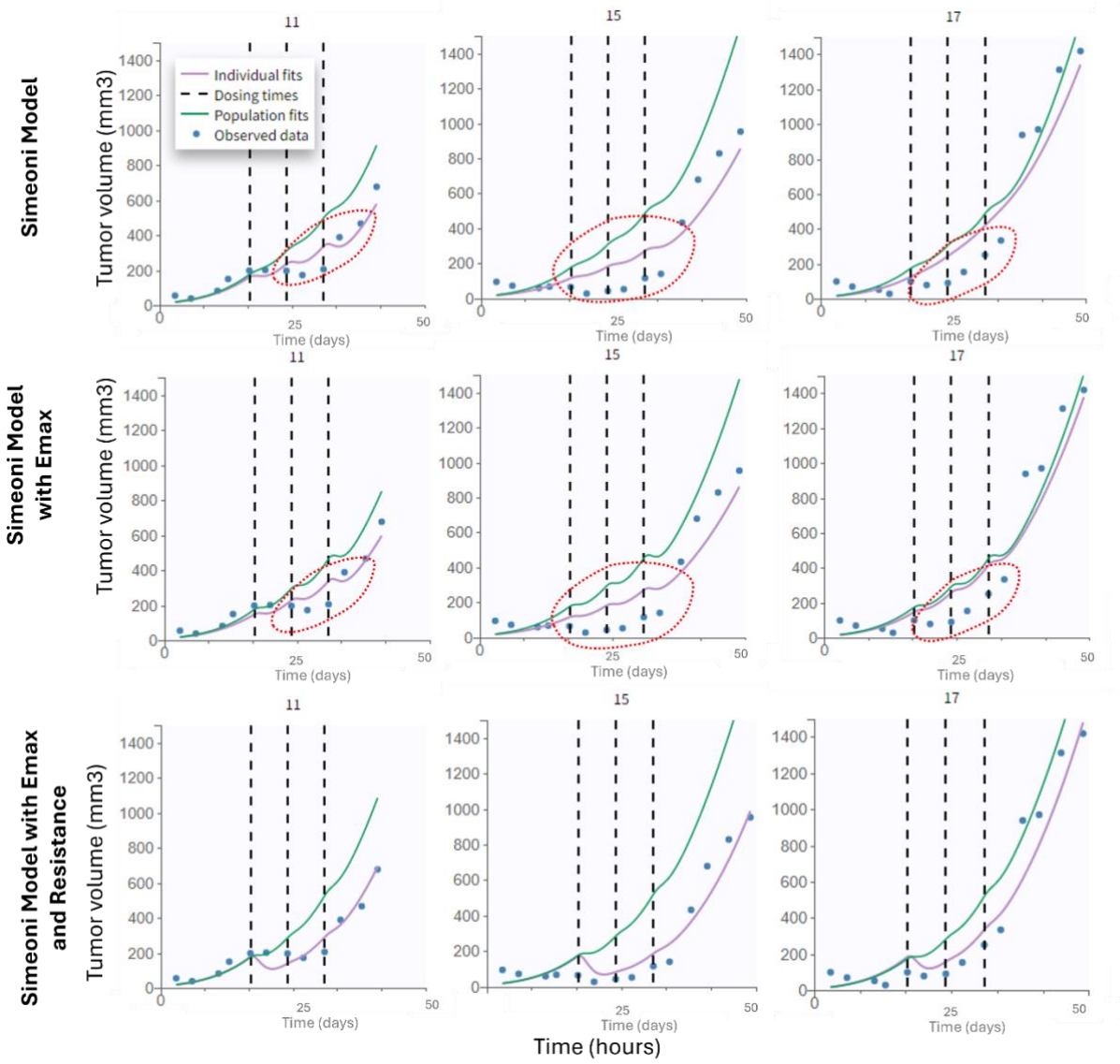

Figure S1. Representation of Individual curves of IV Ptx group for three individuals chosen randomly for Simeoni Model (top row), Simeoni with E_{max} Model (middle row) and Simeoni with E_{max} and resistance Model (bottom row) models. Misspecifications were circled in red. Purple and green lines represent individual and population fits, respectively. Dotted black lines represent the dosing time of Ptx treatments and observations are represented with blue dots.

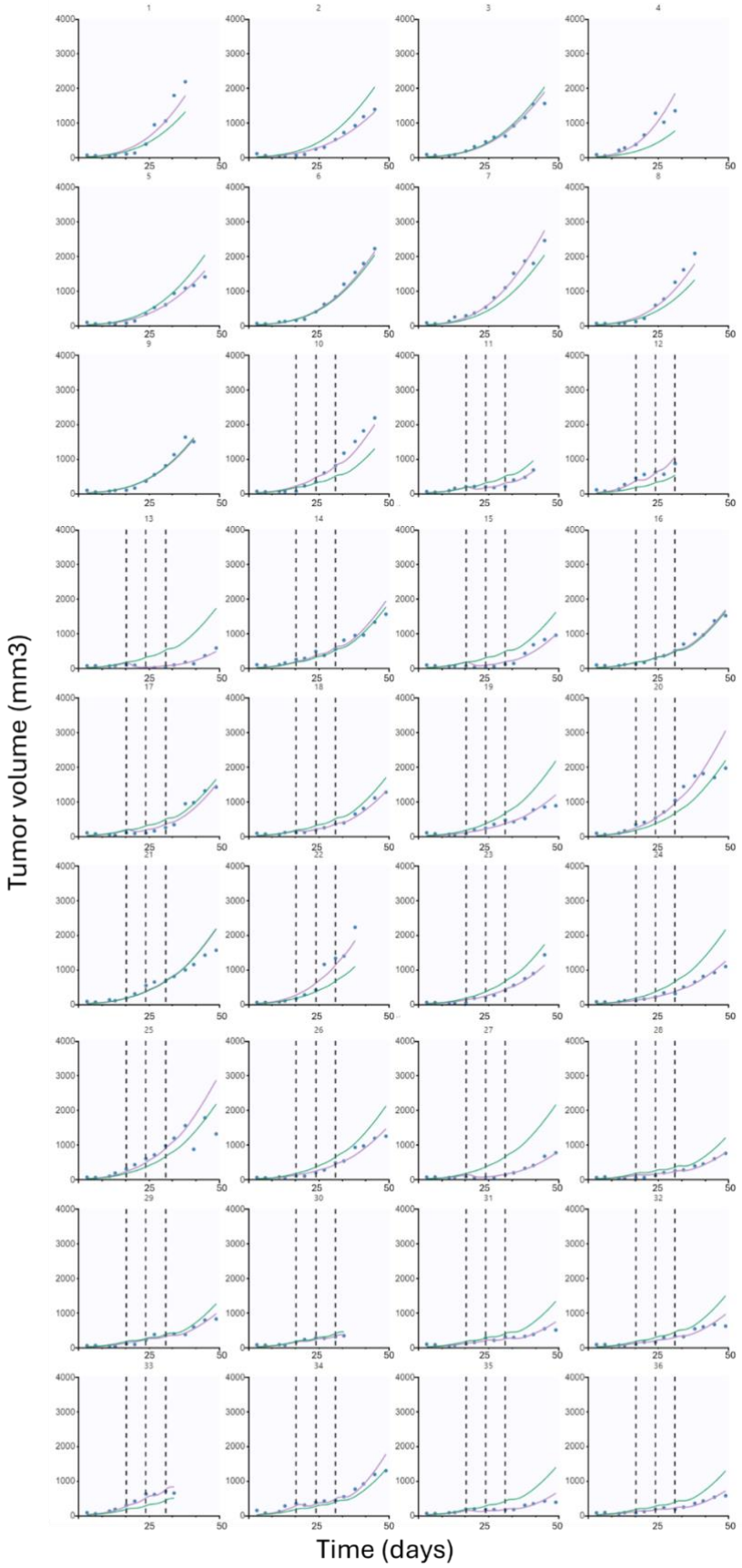

Figure S2. Representation of Individual fit with the final Model of PAAm 60 mg/kg eq. control group (Individual 1-9), IV Ptx group (Individual 10-18), SC Ptx-PAAm 15 mg/kg group (Individual 19-27) and SC Ptx-PAAm 60 mg/kg group (Individual 28-36). Purple and green lines represent individual and

population fits, respectively. Dotted black lines represent the dosing time of Ptx treatments and observations are represented with blue dots.

Table S2. Final PK and PD parameter estimates for IV Ptx and SC Ptx-PAAm implementing all available data (i.e., SC PAAm acting 60 mg/kg eq. as control, IV Ptx 15 mg/kg, SC Ptx-PAAm 15 mg/kg and SC Ptx-PAAm 60 mg/kg). RSE (Relative standard error) is a measure of the precision of the parameter estimates, expressed as coefficient of variation (CV%); Ω is the standard deviation estimated to describe inter-animal variability using Monolix® software.

PARAMETER (UNITS)	ESTIMATE	RSE %
FIXED EFFECT		
V1 (mL)	10.73	5.82
K_{12} (h^{-1})	0.65	12.8
K_{21} (h^{-1})	0.51	0.0852
K_e (h^{-1})	2.76	0.134
K_b (h^{-1})	0.047	13.5
γ	7.17	5.25
β (h^{-1})	0.0013	10.3
Ktran (h^{-1})	0.05	0.402
E_{max1}(h^{-1})	15.48	40.1
E_{max2} (h^{-1})	13.8	3.51
EC50 (μg/mL)	462.7	1.16
STANDARD DEVIATION OF THE RANDOM EFFECT		
ΩV1	0.26	19.4
ΩK_{12}	0.21	37
ΩK_b	0.57	19.9
Ω$K_β$	0.14	24.5

$\boldsymbol{\Omega E_{max1}}$	1.23	25.4

Table S3. Summary of all the PK and PD models tested. PK = Pharmacokinetics, D = dose (µg/mL), A_i = amount of drug in compartment i (µg), C = free concentration of Ptx in the central compartment (µg/mL) = A_i / V, V = volume of distribution (mL), V_m = maximum elimination rate (mL/h), k_m = Michaelis-Menten constant (µg), k_{ij} = distribution rate constant from compartment i to compartment j (1/h), k_e = elimination rate constant (1/h), k_a = absorption rate constant (1/h), T_{lag} = lag time (h), TV = tumor volume (mm^3), TV_0 = initial tumor volume (i.e., 10 mm^3, because 10 millions of cells were first inoculated), t = time (h), RE = random effect, G = growth term (= one untreated tumor growth model), ive = initial value of the estimates before identification.

Model Name	Model purpose	Equation	Comments	Ref
IV - One compartment model - linear elimination	**PK**	$\frac{dA_1}{dt} = -k_e.A_1$	$t\_0 = 0$ $A_1\_0 = \frac{D}{V}$	[46]
IV - Two compartment model - linear elimination	**PK**	$\frac{dA_1}{dt} = -k_e.A_1 - k_{12}.A_1 + k_{21}.A_2$ $\frac{dA_2}{dt} = k_{12}.A_1 - k_{21}.A_2$	$t\_0 = 0$ $A_1\_0 = \frac{D}{V}$ $A_2\_0 = 0$	[46]
IV - Three compartment model - linear elimination	**PK**	$\frac{dA_1}{dt} = -k_e.A_1 - k_{12}.A_1 + k_{21}.A_2 - k_{13}.A_1 + k_{31}.A_3$ $\frac{dA_2}{dt} = k_{12}.A_1 - k_{21}.A_2$ $\frac{dA_3}{dt} = k_{13}.A_1 - k_{31}.A_3$	$t\_0 = 0$ $A_1\_0 = \frac{D}{V}$ $A_2\_0 = 0$ $A_3\_0 = 0$	[46]
IV - Two compartment model – nonlinear elimination	**PK**	$\frac{dA_1}{dt} = -\frac{\frac{V_m}{V}.A_1}{K_m + A_1} - k_{12}.A_1 + k_{21}.A_2$ $\frac{dA_2}{dt} = k_{12}.A_1 - k_{21}.A_2$	$t\_0 = 0$ $A_1\_0 = \frac{D}{V}$ $A_2\_0 = 0$	[46]
Two compartment model - linear - elimination – lag time	**PK**	$\frac{dA_1}{dt}(t) = -k_e.A_1(t - T_{lag}) - k_{12}.A_1(t - T_{lag}) + k_{21}.A_2(t)$ $\frac{dA_2}{dt}(t) = k_{12}.A_1(t) - k_{21}.A_2(t)$	$t\_0 = 0$ $A_1(t < 0) = 0$ $A_1\_0 = \frac{D}{V}$ $A_2\_0 = 0$	[46]
SC - Two compartme	**PK**	$\frac{dA_a}{dt} = -k_a.A_a$	$t_0 = 0$ $A_a\_0 = 0$ $A_1\_0 = 0$	[46]

nt model - linear elimination		$\frac{dA_1}{dt} = k_a.A_a - k_e.A_1 - k_{12}.A_1 + k_{21}.A_2$ $\frac{dA_2}{dt} = k_{12}.A_1 - k_{21}.A_2$	$A_2\_0 = 0$	
Exponential	Untreated tumor growth	$\frac{dTV}{dt} = \lambda . \mathrm{TV}$	$TV\_0 = 10$	[47]
Power Law	Untreated tumor growth	$\frac{dTV}{dt} = \alpha . \mathrm{TV}^{\gamma}$	*TV_0 = 10*	[48]
Logistic	Untreated tumor growth	$\frac{dTV}{dt} = \lambda . \mathrm{TV} . \left(1 - \frac{TV}{TVmax}\right)$	*TV_0 = 10*	[49]
Gompertz	Untreated tumor growth	$\frac{dTV}{dt} = \alpha . \exp\left((-\beta . \mathrm{t})\right). \mathrm{TV}$	*TV_0 = 10*	[50]
Reduced Gompertz	Untreated tumor growth	$\frac{dTV}{dt} = (\beta . \gamma) - \beta . \log\left(\frac{TV}{TV_0}\right). \mathrm{TV}$	*TV_0 = 10*	[20]
Simeoni	Drug effect	$\frac{dTV_1}{dt} = G - ktran . C . TV_1$ $\frac{dTV_2}{dt} = ktran . C . TV_1 - ktran . TV_2$ $\frac{dTV_3}{dt} = ktran . (TV_2 - TV_3)$ $\frac{dTV_4}{dt} = ktran . (TV_3 - TV_4)$	$TV = TV_1 + TV_2 + TV_3 + TV_4$ *TV_0 = 10* *TV_1_0 = 0* *TV_2_0 = 0* *TV_3_0 = 0*	[19]
Norton Simon	Drug effect	$\frac{dTV}{dt} = G - (e . C . e^{(-\beta . \gamma . \mathrm{t})} TV)$	$TV\_0 = 10$	[51]
Log Kill	Drug effect	$\frac{dTV}{dt} = G - e . C . TV$	*TV_0 = 10*	[52]
Threshold killing	Drug effect	if $C < Cmin$: $\frac{dTV}{dt} = G$ else: $\frac{dTV}{dt} = G - (e . (C - Cmin) . TV$	$TV\_0 = 10$	[34]